Top Catal (2015) 58:613–622
DOI 10.1007/s11244-015-0403-z

ORIGINAL PAPER

CH_3CH_2OH, CD_3CD_2OD, and CF_3CH_2OH Decomposition on ZnO$(1\bar{1}00)$

Aaron Reinicker[1] · James B. Miller[1] · Wooseok Kim[2] · Kijung Yong[2] · Andrew J. Gellman[1]

Published online: 6 June 2015

Abstract The decomposition of CH_3CH_2OH, CD_3CD_2OD, and CF_3CH_2OH on Zn$(1\bar{1}00)$ was studied using temperature programmed reaction spectroscopy. $CH_3CH{=}O$ ($CD_3CD{=}O$, $CF_3CH{=}O$), $CH_2{=}CH_2$ ($CD_2{=}CD_2$, $CF_2{=}CH_2$), H_2O (D_2O) and H_2 (D_2) were formed in all cases. The CH_3CH_2OH decomposition mechanism includes the formation of two intermediate species on the surface: CH_3CH_2- bonded to surface lattice O atoms decomposes to form $CH_2{=}CH_2$ while CH_3CH_2O– bonded to surface Zn atoms decomposes to form $CH_3CH{=}O$. A significant isotope effect observed for the formation of $CH_2{=}CH_2$ versus $CD_2{=}CD_2$ suggests that C–H(D) bond breaking at the β-carbon is the rate-limiting step in CH_3CH_2– (CD_3CD_2–) decomposition. Decomposition of CF_3CH_2OH leaves F-atoms on the surface as a result of β-fluoride elimination in CF_3CH_2–. A significant F substituent effect in desorption of $CF_3CH{=}O$ versus $CH_3CH{=}O$ indicates that the CF_3 group increases the barrier to the β-hydride elimination step yielding $CF_3CH{=}O$ and suggests that the transition state is cationic, $C^{\delta+}\cdots H^{\delta-}$.

Keywords ZnO · Ethanol · Temperature progress · Reaction spectroscopy · Kinetic isotope effect · Substituent effect

Electronic supplementary material The online version of this article (doi:10.1007/s11244-015-0403-z) contains supplementary material, which is available to authorized users.

✉ Andrew J. Gellman
gellman@cmu.edu

[1] Department of Chemical Engineering, Carnegie Mellon University, Pittsburgh, PA 15213, USA

[2] Department of Chemical Engineering, Pohang University of Science and Technology, Gyeongsangbuk-do, South Korea

1 Introduction

ZnO is a wide band-gap II–VI semiconductor that has applications in blue and UV LEDs, solar cells, catalysts, and chemiresistive sensors [1–5]. ZnO has a hexagonal ("wurtzite") structure and can expose a variety of crystal facets, each with its own unique surface chemistry [6–9]. For sensor and catalytic applications of nanoscale ZnO morphologies, there has been recent interest in one-dimensional "nanorod" structures, which have high surface-to-volume ratios [2]. ZnO nanorods grow preferentially along their *c*-axes, and most of their exposed surface area is composed of "non-polar" ZnO{1100} planes, with equal densities of surface O and Zn atoms. Characterization of the interactions of typical analyte and reactant species with these ZnO{1100} surfaces is important for understanding and improving ZnO-based sensors and catalysts.

A number of studies of alcohol adsorption and reaction on single crystal ZnO surfaces have been published [6, 10–12]. Mokwa et al. reported H_2, H_2O, $CH_3CH{=}O$, and $CH_2{=}CH_2$ as the primary products of thermal decomposition of CH_3CH_2OH on non-polar ZnO$(1\bar{1}00)$ [6]. Shao et al. used scanning tunneling microscopy (STM) to study the intermediates formed by CH_3OH adsorption at 300 K on ZnO$(1\bar{1}00)$ [13]. They observed two different surface species on the ZnO$(1\bar{1}00)$ surface; a methyl (–CH_3) species formed at a surface lattice O site upon breakage of the C–O bond in CH_3OH, and a methoxy (CH_3O–) species formed at a surface lattice Zn site upon breaking of the O–H bond. DFT calculations confirmed that the formation of both species was energetically favorable by −0.8 eV for CH_3O– formation and −0.4 eV for –CH_3 formation.

While the products of CH_3CH_2OH decomposition on the ZnO$(1\bar{1}00)$ surface have been identified, little is known

about the details of the reaction mechanism or its transition state(s). In this work, we use temperature programmed reaction spectrometry (TPRS) to examine the thermal decomposition of CH_3CH_2OH, CD_3CD_2OD and CF_3CH_2OH on ZnO($1\bar{1}00$). We propose a reaction mechanism and surface intermediate species that are consistent with the observed decomposition products. Deuterium kinetic isotope effects and F substitution effects observed in TPRS of CD_3CD_2OD and CF_3CH_2OH, respectively, provide insight into the rate limiting steps and the transition states in the mechanisms for formation of $CH_3CH{=}O$ and $CH_2{=}CH_2$ during CH_3CH_2OH decomposition on ZnO($1\bar{1}00$). The reaction products, F substituent effects and kinetic isotope effects are consistent with a mechanism for CH_3CH_2OH decomposition on ZnO($1\bar{1}00$) in which there are two parallel pathways through two distinct intermediates; an ethoxy (CH_3CH_2O–) intermediate bound to the Zn sites and leading to the formation of $CH_3CH{=}O$ and an ethyl (CH_3CH_2–) intermediate bound to the lattice O sites and leading to the formation of $CH_2{=}CH_2$.

2 Experimental

Experiments were performed in an ultra high vacuum (UHV) chamber with a base pressure of 3×10^{-10} Torr equipped with an Omicron NSE 10 ion gun for Ar^+ ion sputter cleaning of the ZnO surface; a Dycor quadrupole mass spectrometer for identification and quantification of desorption products; a Specs x-ray source and an Omicron EA125 hemispherical analyzer for performing X-ray Photoelectron Spectroscopy (XPS); a leak valve for introduction of ethanol vapor into the chamber background; and a PHI low energy electron diffraction (LEED) optics.

A $10 \times 10 \times 1$ mm^3 ZnO($1\bar{1}00$) single crystal was bonded to a Ta plate using Aremco Pyroduct 597-A, a thermally and electrically conducting Ag based paste. Two Ta wires were spot-welded to the Ta plate and then attached to the end of a sample manipulator mounted vertically in the UHV chamber. The crystal mount was in thermal contact with a liquid N_2 reservoir and the Ta plate was heated resistively to reach temperatures in the range 100–1000 K. The temperature was measured using a K-type thermocouple spot-welded to the Ta plate and was controlled using a computer.

Before each TPRS experiment, the ZnO($1\bar{1}00$) crystal was prepared by at least two cycles of (1) sputtering at 400 K with a 6 μA current of 2 kV Ar^+ ions for 50 min and (2) annealing for 5 min at 750 K. XPS analysis verified the cleanliness and the Zn:O atomic ratio of the surface. LEED verified that the surface retained its Zn($1\bar{1}00$) order after the sputtering and annealing cycles (Figure S1 of the Supplementary Information) [14]. CH_3CH_2OH (99.6 %, Sigma-Aldrich), CD_3CD_2OD (99.5 %, Sigma-Aldrich), and CF_3CH_2OH (>99 %, Sigma-Aldrich) were purified by several freeze–pump–thaw cycles before introduction into the chamber via a leak valve for background exposure of the ZnO($1\bar{1}00$) surface at 300 K.

XPS characterization of the ZnO($1\bar{1}00$) crystal was performed using an Al K_α x-ray source and a seven channeltron Omicron EA 125 hemispherical energy analyzer operated with a pass energy of 100 eV in constant analyzer energy (CAE) mode. The sample was positioned 5 mm in front of the x-ray source, oriented at an angle midway between the axes of the x-ray source and the lens of the hemispherical energy analyzer. This angle and sample position yielded the maximum Zn $2p_{3/2}$ signal. Integrated areas of the Zn$2p_{3/2}$, O1s, F1s, and C1s peaks were used with Wagner library sensitivity factors for quantitative estimates of surface compositions [15].

TPRS experiments were performed using the quadrupole mass spectrometer to monitor species that desorbed from the ZnO($1\bar{1}00$) surface. After exposure to CH_3CH_2OH, CD_3CD_2OD, or CF_3CH_2OH, the ZnO($1\bar{1}00$) crystal was positioned in front of the mass spectrometer <5 mm from the aperture to the ionizer and then heated from 300 to 700 K at 1 K/s in each TPRS experiment. The mass spectrometer signal for any given *m/z* contains contributions from multiple desorbing species and cannot be used to directly determine the relative yields of product species desorbing into the gas phase. Therefore, the mass spectrometer signals from each TPRS experiment were converted to pressures by determining the signal intensities at each *m/z* for each pure component species introduced into the chamber at a known pressure. Pure CH_3CH_2OH, $CH_3CH{=}O$, H_2, H_2O, or $CH_2{=}CH_2$ were leaked into the UHV chamber at pressures between 1×10^{-9} Torr and 5×10^{-8} Torr, measured using a Bayard-Alpert ion gauge corrected for sensitivity [16], and the signals at $m/z = 2$, 18, 28, 29, and 31 were recorded. For each of the five pure components, *i*, introduced into the chamber, the mass spectrometer signals at 5 *m/z* ratios, *j*, were measured at 4 different pressures, $I_{ij}(P)$. The sensitivity of signal to pressure was calculated to yield $\alpha_{ij} = \frac{dI_{ij}}{dP}$. This was repeated for the five pure components to create a 5×5 matrix, $\overline{\overline{\alpha}}$. A similar matrix was developed for TPRS of CD_3CD_2OD by leaking pure D_2, D_2O, $CD_3CD{=}O$, $CD_2{=}CD_2$, or CD_3CD_2OD into the UHV chamber at pressures between 1×10^{-9} Torr and 5×10^{-8} Torr and recording signals at $m/z = 4$, 20, 32, 30, and 34. The $\overline{\overline{\alpha}}$ matrices for CH_3CH_2OH and CD_3CD_2OD decomposition products are given in Tables S1 and S2, respectively, of the Supplementary

Information. These matrices were used to convert the TPRS signals at the five *m/z* ratios into pressures of each component desorbing from the surface. This analysis was not applied to TPRS experiments of CF_3CH_2OH due to the lack of availability of all pure component products of CF_3CH_2OH decomposition.

3 Results

3.1 XPS of Clean ZnO$(1\bar{1}00)$ and CH_3CH_2OH/ZnO$(1\bar{1}00)$

XP spectra of the sputtered and annealed ZnO$(1\bar{1}00)$ surface were acquired before TPRS to verify surface cleanliness and surface composition. The ratio of Zn:O was 0.95 ± 0.05, as determined from 20 cleaned surfaces. Figure 1 shows the C1s signal from the ZnO$(1\bar{1}00)$ surface before dosing, after a CH_3CH_2OH exposure of 0.4 L (sufficient to saturate the surface at 300 K), and after TPRS of the adsorbed CH_3CH_2OH. A small C1s peak, equivalent to <1 % of the surface composition, is visible in the XPS of the clean surface at 282 eV. The C content of the surface was <1 % (atomic) before each TPRS experiment. After exposure of the surface to 0.4 L of CH_3CH_2OH, a larger C1s feature, corresponding to a saturated monolayer of CH_3CH_2OH, is observed at a binding energy of 283.5 eV. After TPRS of the adsorbed CH_3CH_2OH, the C 1 s signal decreases significantly to ~15 % of its original intensity, indicating that ~85 % of the CH_3CH_2OH monolayer desorbed or decomposed into gas phase products.

3.2 Products of CH–$_3CH_2OH$/ZnO$(1\bar{1}00)$ TPRS

To identify the products of CH_3CH_2OH decomposition on the ZnO$(1\bar{1}00)$ surface, a series of TPRS experiments were performed after exposure of the ZnO$(1\bar{1}00)$ surface to 0.4 L of CH_3CH_2OH at 300 K, an exposure that saturates the CH_3CH_2OH monolayer without leading to multilayer adsorption. TPRS was conducted by heating the surface from 300 to 700 K at 1 K/s while monitoring desorption signals at *m/z* ratios of 2, 18, 28, 29 and 31 with the mass spectrometer. The *m/z* ratios monitored were chosen based on species identified in previously published reports of CH_3OH and CH_3CH_2OH decomposition on a variety of ZnO surfaces [7, 8, 17, 18]. The species identified desorbing from the surfaces in those studies include: CO, CO_2, CH_4, CH_2=CH_2, CH_3CH_3, O_2, H_2, CH_3CH=O, H_2O, and CH_3CH_2OH. Among these, the primary CH_3CH_2OH decomposition products observed in our TPRS experiments were H_2, H_2O, CH_2=CH_2, CH_3CH=O, and CH_3CH_2OH.

Figure 2 displays the TPR spectra obtained following a 0.4 L exposure of CH_3CH_2OH to ZnO$(1\bar{1}00)$ at 300 K. The product desorption curves are displayed as pressures of H_2, H_2O, CH_2=CH_2, CH_3CH=O, and CH_3CH_2OH. The baselines of the spectra have been offset for clarity in Fig. 2. For H_2O, there is a sharp peak at 355 K with two lower intensity peaks at 440 and 550 K. For CH_2=CH_2 there is a low temperature feature at 380 K with a broad peak at 480 K. For CH_3CH=O desorption, there is a broad peak between 400 and 550 K. For H_2, there is a broad desorption feature centered at 480 K, starting at 420 K and ending at 570 K; for CH_3CH_2OH there is a large desorption feature at 375 K with a smaller shoulder at 440 K. The

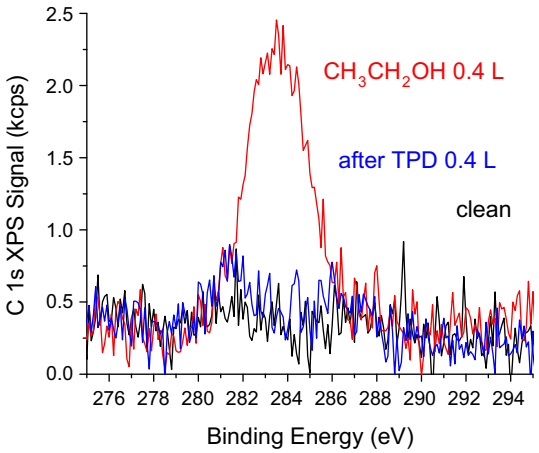

Fig. 1 C1s XP spectra of the ZnO$(1\bar{1}00)$ surface after cleaning, after exposure to 0.4 L of CH_3CH_2OH at 300 K, and after thermal decomposition of the adsorbed CH_3CH_2OH during heating to 700 K at 1 K/s. Baselines were subtracted from all three spectra. Over 85 % of the adsorbed CH_3CH_2OH and its decomposition products desorb during TPRS, with ~15 at% C remaining on the ZnO$(1\bar{1}00)$ surface

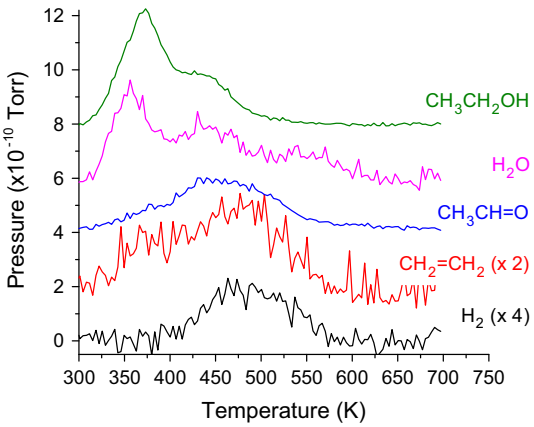

Fig. 2 TPRS of CH_3CH_2OH (exposure of 0.4 L) on ZnO$(1\bar{1}00)$. The pressure of each species was calculated from the mass spectral signal versus temperature for $m/z = 2$, 18, 28, 29, and 31 using the $\bar{\bar{\alpha}}$ matrix described in the experimental section and given in Table S1 of the Supplementary Information. Backgrounds were subtracted from each spectrum before plotting and the spectra have been offset for clarity

noise in the TPR spectra of H_2, H_2O, and CH_2=CH_2 is larger than for CH_3CH=O and CH_3CH_2OH because of contributions of the background signals at $m/z = 2$, 18, and 28 from the H_2, H_2O and CO in the background of the UHV chamber.

TPR spectra of CH_3CH=O and CH_3CH_2OH, after CH_3CH_2OH exposures in the range 0.005–30 L, are shown in Fig. 3. Note that CH_2=CH_2 desorption is also observed after exposure of ZnO(1$\bar{1}$00) to CH_3CH_2OH, but is not shown in Fig. 3 because the signal at $m/z = 28$ amu is quite noisy due to its overlap with that of CO in the UHV chamber. At exposures $\leq$0.05 L, a broad CH_3CH=O desorption peak is observed from 400 to 525 K, and there is no significant CH_3CH_2OH desorption. For exposures $\geq$0.4 L, the desorption signals for both CH_3CH=O and CH_3CH_2OH saturate. From exposures of 0.05 to 0.4 L, the CH_3CH_2OH desorption increases significantly. This pattern suggests that at low coverages CH_3CH_2OH initially populates sites or adsorption states that result in CH_3CH_2OH decomposition to yield CH_3CH=O formation.

To estimate the peak locations and widths of multiple TPRS features, Lorentzian curves were fit to the pressure versus temperature data (see Supplementary Information Figures S2 and S3 for examples). Two distinct features are present in the desorption spectrum of CH_3CH_2OH, one centered at 370 K and a second at 438 K. Whether these arise from desorption of molecularly adsorbed CH_3CH_2OH or from recombination of CH_3CH_2O and H atoms, is not determined. There are also two features in the desorption spectrum of CH_3CH=O, peaks at 435 and 495 K.

3.3 Products of CD_3CD_2OD/ZnO(1$\bar{1}$00) TPRS

TPR spectra following various CD_3CD_2OD exposures to ZnO(1$\bar{1}$00) were acquired at the same conditions as used for the CH_3CH_2OH experiments. Figure 4 shows TPRS spectra for a 0.4 L exposure of CD_3CD_2OD at 300 K as pressures of D_2, D_2O, CD_3CD=O, CD_2=CD_2, and CD_3CD_2OD. The raw signal versus temperature for $m/z = 4$, 20, 32, 30, and 34 were converted to product pressures using the $\bar{\bar{\alpha}}$ matrix in Table S2 of the Supplementary Information. The baseline pressure of each spectrum is zero; however, they have been offset for clarity in Fig. 4. The desorption and decomposition of CD_3CD_2OD on ZnO(1$\bar{1}$00) follow the same general trends as those for CH_3CH_2OH. The main feature for D_2O desorption appears at 360 K, roughly the same temperature as for H_2O desorption observed during CH_3CH_2OH TPRS. D_2O also displays lower intensity, higher temperature desorption peaks at 450 and 550 K much like H_2O during CH_3CH_2OH TPRS. The CD_3CD_2OD desorption spectrum has a peak at 370 K, with a shoulder at 440 K, roughly the same temperatures as for CH_3CH_2OH. CD_3CD=O desorption has a low temperature shoulder at 435 K, with a high temperature feature at 490 K. The CD_2=CD_2 desorption spectrum has a peak at 500 K, $\sim$20 K higher than that observed for CH_2=CH_2 during CH_3CH_2OH TPRS. D_2 desorption displays a peak at 505 K, 20 K higher than that of H_2 from CH_3CH_2OH.

Figure 5 displays CD_3CD_2OD, CD_3CD=O, and CD_2=CD_2 desorption spectra for CD_3CD_2OD exposures from 0.006 to 3 L. Desorption of both CD_3CD=O and CD_2=CD_2 occurs at low exposures, indicating that CD_3CD_2OD initially populates the sites or states that result in CD_3CD_2OD decomposition to these two products. The amount of both CD_3CD=O and CD_2=CD_2 that desorbs increases with increasing exposure. CD_3CD_2OD does not desorb at exposures <0.05 L; for higher exposures, the CD_3CD_2OD desorption yield increases with increasing exposure until the surface becomes saturated by an exposure of $\sim$0.4 L. This is the same trend as was observed for CH_3CH_2OH/ZnO(1$\bar{1}$00) TPRS. Peaks were fit to the CD_3CD_2OD

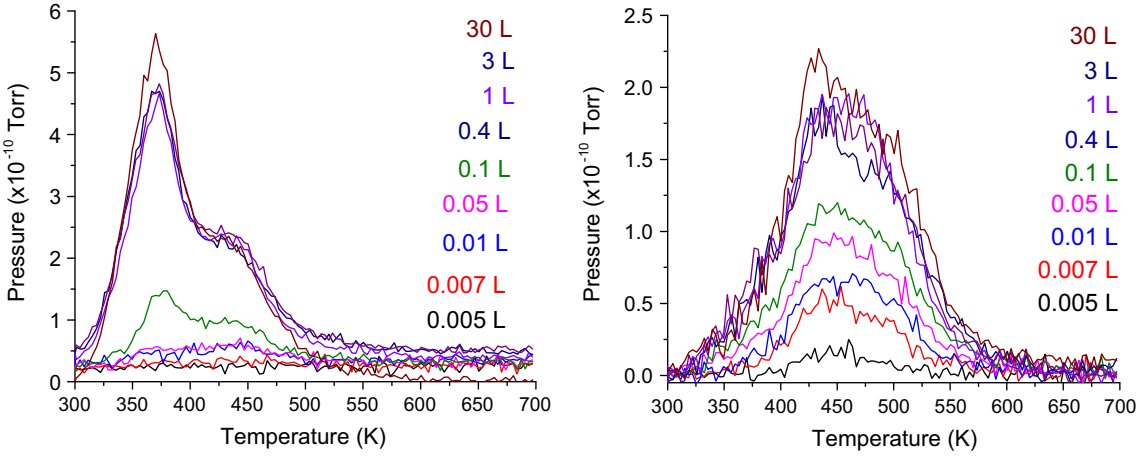

Fig. 3 TPRS of CH_3CH_2OH (*left*) and CH_3CH=O (*right*) following various exposures of CH_3CH_2OH to the ZnO(1$\bar{1}$00) surface. CH_3CH=O desorption increases with increasing exposure; CH_3CH_2OH desorption is not significant until the exposure reaches 0.1 L

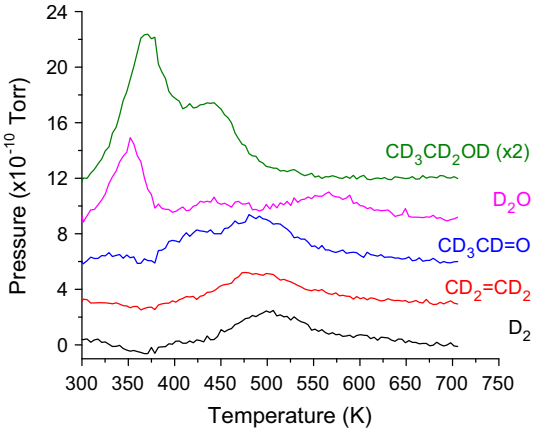

Fig. 4 TPR spectra of a 0.4 L exposure of CD_3CD_2OD on ZnO(1$\bar{1}$00). The spectra have been offset for clarity. The pressure of each species was calculated from the raw data of signal versus temperature for $m/q = 4$, 20, 32, 30, and 34 using the $\bar{\bar{\alpha}}$ matrix described in the experimental section. The peak locations follow a similar pattern to TPRS of CH_3CH_2OH

spectra using the same Lorentzian peak fitting as for CH_3CH_2OH (a graphical display of a typical fit appears in Figure S3 of the Supplementary Information.) The spectrum of $CD_3CD=O$ is best fit by two Lorentzian peaks centered at 432 and 491 K. The TPR spectrum of $CD_2=CD_2$ is best fit by one peak centered at about 490 K. Because there is a large CD_3CD_2OD desorption feature at 375 K (see Fig. 5), it is possible that the 375 K feature for $CD_2=CD_2$ after a 0.1 L exposure can be traced to CD_3CD_2OD contributions that were not completely subtracted from the spectra. This 375 K feature was only present in the 0.1 and 0.05 L exposures of CD_3CD_2OD.

3.4 Products of CF_3CH_2OH/ZnO(1$\bar{1}$00) TPRS

TPR spectra of CF_3CH_2OH adsorbed on ZnO(1$\bar{1}$00) were acquired at the same conditions as were used for the CD_3CD_2OD and CH_3CH_2OH experiments. Figure 6 (left) shows TPR spectra after exposure of 0.4 L of CF_3CH_2OH at 300 K. Desorption products from TPRS of CF_3CH_2OH were similar to those observed for CD_3CD_2OD and CH_3CH_2OH; they included $m/z = 18$ (H_2O), 29 ($CF_3CH=O$), 31 (CF_3CH_2OH), and 45 ($CF_2=CH_2$). The signal for $m/z = 2$ (H_2) was too small to be measured. The TPRS signal at $m/z = 18$ follows a trend similar to those of H_2O and D_2O from CH_3CH_2OH and CD_3CD_2OD, but with peaks shifted to ~30 K higher temperatures: the $m/z = 18$ spectrum has a peak at 380 K, with a shoulder extending to 650 K. The peak for $m/z = 45$ for $CF_2=CH_2$ desorption starts at 325 K and ends at 525 K. Both $m/z = 29$ and $m/z = 31$ result from ionization of CF_3CH_2OH, where $m/z = 31$ is the highest intensity signal and $m/z = 29$ signal has 60 % relative intensity; both TPRS features are broad. The broad peak for $m/z = 31$ after a 0.4 L exposure shows that the parent molecule, CF_3CH_2OH, desorbs from the surface. At exposures ≤0.1 L the signal from $m/z = 29$ is larger than the signal from $m/z = 31$ suggesting that there is some limiting coverage of adsorbed species below which $CF_3CH=O$ and $CF_2=CH_2$ are the major reaction products (see Figure S4 of the Supplementary Information). Once surface sites for $CF_2=CH_2$ and $CF_3CH=O$ formation are saturated, CF_3CH_2OH desorption occurs either through molecular desorption or recombinative desorption.

To isolate a net signal for $CF_3CH=O$, the contribution from CF_3CH_2OH was subtracted from the signal at $m/z = 29$. Figure 6 (right) compares $CF_2=CH_2$ desorption and CF_3CH desorption for a 0.4 L exposure of CF_3CH_2OH; the peak locations differ by over 100 K. The major species formed after high exposures of CF_3CH_2OH are H_2O and CF_3CH_2OH, while at lower exposures $CF_3CH=O$ and $CF_2=CH_2$ are more prominent than CF_3CH_2OH. The products and desorption trends from CF_3CH_2OH are consistent with those from TPRS of both CH_3CH_2OH and CD_3CD_2OD on ZnO(1$\bar{1}$00).

XPS was used to determine the state of the ZnO(1$\bar{1}$00) surface after each TPRS experiment was performed. Figure 7 shows the F 1 s XPS spectral region for the clean ZnO(1$\bar{1}$00) and after TPRS of a 0.4 L exposure of CF_3CH_2OH. The clean surface displays no evidence of F. After TPRS, there is a peak for F bonded to Zn at a binding energy of 684 eV in the F1s spectrum [15]. The XPS characterization was not performed before the TPRS experiment to eliminate the possibility of x-ray induced dissociation of F from CF_3CH_2OH. Residual surface F after the TPRS experiment must, therefore, come from a surface reaction and not from x-ray induced dissociation. XPS was also performed for a 0.4 L exposure of CF_3CH_2OH at 300 K on ZnO(1$\bar{1}$00) in a separate experiment to determine the fraction of F deposited on the surface by the decomposition reaction. The F1s signal in Fig. 7 is ~25 % of the F 1 s signal of the 0.4 L exposure of CF_3CH_2OH at 300 K meaning that 25 % of the adsorbed CF_3CH_2OH deposits F onto the surface as a result of $CF_2=CH_2$ formation or decomposition by other pathways.

4 Discussion

4.1 Mechanism of CH_3CH_2OH Decomposition on ZnO(1$\bar{1}$00)

In order to elucidate the mechanism of CH_3CH_2OH decomposition on ZnO(1$\bar{1}$00), we have attempted to quantify the stoichiometry of the product yield. Table 1 lists the fractional yields of the products of CH_3CH_2OH and CD_3CD_2OD decomposition for exposures that yield

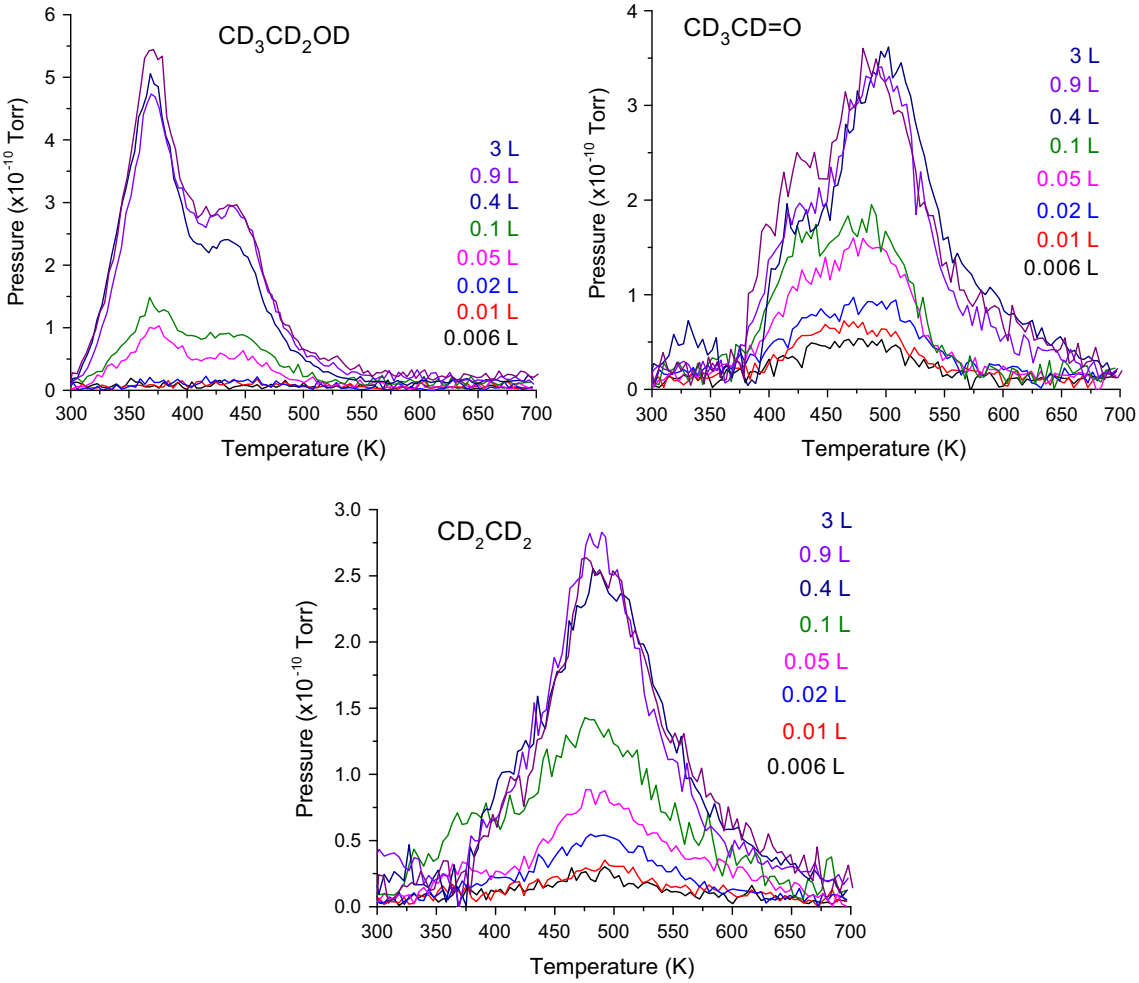

Fig. 5 TPR spectra of CD_3CD_2OD, $CD_3CD{=}O$, and $CD_2{=}CD_2$ desorption from ZnO($1\bar{1}00$) after various exposures of CD_3CD_2OD. Peaks for $CD_3CD{=}O$ and $CD_2{=}CD_2$ desorption are present even at low exposures and increase with increasing exposure. CD_3CD_2OD desorption is only observed for exposures ≥0.05 L

saturation coverages of the adsorbed CH_3CH_2OH and CD_3CD_2OD monolayers (≥0.4 L). The pressure fractions were calculated from the TPRS peak areas (after conversion to pressure) of each species. The fractional yield of a single component is equal to its TPRS peak area divided by the sum of the peak areas of all five components.

The uncertainties are the standard deviations of the fractional yields measured in five or six experiments. The yield of reversibly adsorbed CH_3CH_2OH is roughly equal to the fraction that decomposes into $CH_3CH{=}O$ and $CH_2{=}CH_2$. This discussion will focus on the decomposition mechanism of the irreversibly adsorbed CH_3CH_2OH. STM imaging has suggested that dissociative adsorption of CH_3OH on ZnO($1\bar{1}00$) can yield both CH_3O– groups adsorbed to surface Zn atoms and CH_3– groups adsorbed on surface O atoms [13]. The framework for our discussion of CH_3CH_2OH decomposition will be a mechanism that is consistent with the suggestion that there are two decomposition intermediates; CH_3CH_2O–Zn groups that decompose to yield $CH_3CH{=}O$ and CH_3CH_2–O groups that yield $CH_2{=}CH_2$. The distinction between these ethoxy groups is that the former results from dissociation of the O–H bond in CH_3CH_2OH and is bound to a surface Zn atom, while the latter is formed by dissociation of the C-O bond in CH_3CH_2OH to yield an ethyl group adsorbed to a surface O atom. In the latter case the CH_3CH_2OH dissociation yields an OH group, possibly bound to a surface Zn atom. The scheme for decomposition of the CH_3CH_2OH fraction that is irreversible bonded to the surfaces is summarized as follows:

$$CH_3CH_2OH_g \rightarrow CH_3CH_2O - Zn + H \quad (1)$$

$$CH_3CH_2O - Zn \rightarrow CH_3CH = O_g + H \quad (2)$$

$$2H \rightarrow H_{2,g} \quad (3)$$

$$CH_3CH_2OH_g \rightarrow CH_3CH_2 - O + HO \quad (4)$$

$$CH_3CH_2 - O \rightarrow CH_2CH_{2,g} + H \quad (5)$$

$$H + OH \rightarrow H_2O_g \quad (6)$$

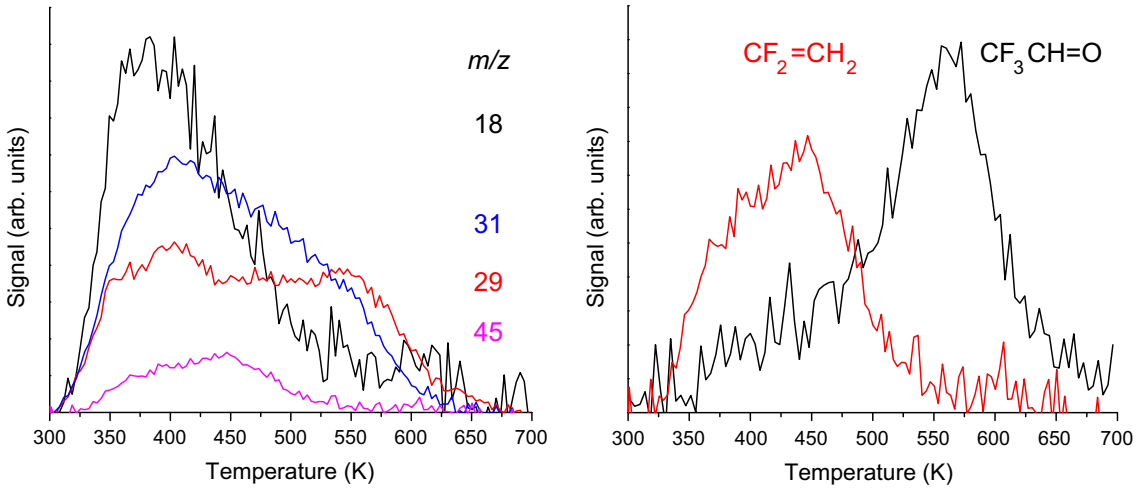

Fig. 6 *Left*: TPRS of a 0.4 L exposure of CF_3CH_2OH to ZnO($1\bar{1}00$). Primary contributors to the signals were H_2O ($m/z = 18$), $CF_3CH{=}O$ (29), $CF_2{=}CH_2$ (45) and CF_3CH_2OH (31). The $m/z = 29$ signal also has a contribution from CF_3CH_2OH. *Right*: Comparison of $CF_3CH{=}O$ desorption and $CF_2{=}CH_2$ desorption. The net signal from $CF_3CH{=}O$ was isolated from the signal at $m/z = 29$ by subtracting the contribution from desorbing CF_3CH_2OH

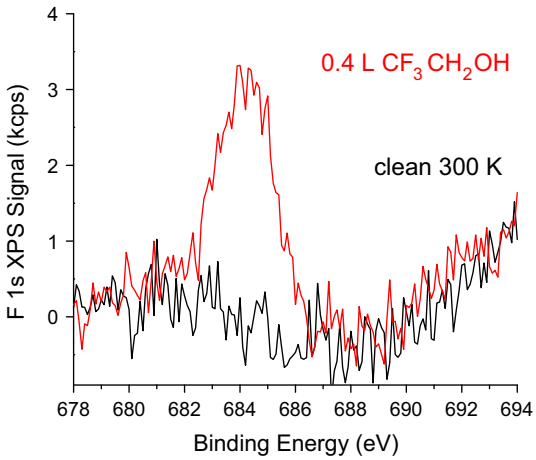

Fig. 7 F 1 s XPS for the clean ZnO($1\bar{1}00$) surface (*black*) and after TPRS of a 0.4 L exposure of CF_3CH_2OH (*red*). Both spectra were baseline subtracted. The clean surface has no peaks in the F1s spectrum. A peak at a binding energy of 684 eV for F bonded to Zn is visible after the TPRS experiment

In this scheme the gas phase species are indicated with a subscript '*g*' and the atoms originated in the ZnO($1\bar{1}00$) surface lattice are boldened. We have been deliberately vague regarding the adsorption sites for the H atoms and OH groups released onto the surface.

The ratio of the yields of $CH_3CH{=}O$ (or $CD_3CD{=}O$) and $CH_2{=}CH_2$ (or $CD_2{=}CD_2$) formed during CH_3CH_2OH (or CD_3CD_2OD) decomposition are roughly equal, although there is nothing that constrains this to be the case. This result is different from that of the STM study of CH_3OH adsorbed on ZnO($1\bar{1}00$), which suggested that the majority surface species was CH_3O–, the precursor to $CH_2{=}O$ formation, while only trace amounts of CH_3–, the precursor to CH_4 formation, were present [13]. The pressure fraction of H_2O evolving from the ZnO($1\bar{1}00$) during CH_3CH_2OH decomposition is significantly larger than that of H_2 and is twice the pressure fraction of $CH_3CH{=}O$ and $CH_2{=}CH_2$. This is an unexpected result. Within the context of the proposed mechanism, the pressure fraction of H_2 should be closer to pressure fraction of $CH_3CH{=}O$ formed. Similarly, the pressure fraction of H_2O formed should be close to that of $CH_2{=}CH_2$. The fractional product yields from CD_3CD_2OD decomposition are similar to those obtained for CH_3CH_2OH. The $CD_2{=}CD_2$ and $CD_3CD{=}O$ yields are roughly equal. As in the case of CH_3CH_2OH decomposition, the yield of D_2 from CD_3CD_2OD is significantly lower than that of D_2O which is slightly higher than that of

Table 1 Product pressure fractions for TPRS of saturated monolayers of CH_3CH_2OH and CD_3CD_2OD on ZnO($1\bar{1}00$)

CH_3CH_2OH products	Pressure fraction	CD_3CD_2OD products	Pressure fraction
H_2	0.05 ± 0.01	D_2	0.04 ± 0.01
H_2O	0.34 ± 0.07	D_2O	0.25 ± 0.06
$CH_3CH{=}O$	0.18 ± 0.04	$CD_3CD{=}O$	0.21 ± 0.07
$CH_2{=}CH_2$	0.17 ± 0.03	$CD_2{=}CD_2$	0.18 ± 0.05
CH_3CH_2OH	0.26 ± 0.05	CD_3CD_2OD	0.3 ± 0.1

CD_2=CD_2. The difference between the yields of CD_2=CD_2 (CD_3CD = O) and CH_2=CH_2 (CH_3CH=O) are not statistically significant.

Based on the products observed, we propose the mechanism for CH_3CH_2OH decomposition described by steps 1–6 listed above. CH_3CH_2OH adsorbs dissociatively via cleavage of either the O–H bond to form CH_3CH_2O– on a surface lattice Zn atom or cleavage of the C–O bond to form CH_3CH_2– on a surface lattice O atom. Roughly half of the adsorbed CH_3CH_2OH desorbs as ethanol. Whether it is adsorbed intact or desorbs as a result of the recombination of CH_3CH_2O– and H is not determined. The irreversibly adsorbed CH_3CH_2O– and CH_3CH_2– decompose by β-hydride elimination to yield CH_3CH=O and CH_2=CH_2, respectively. In this terminology the H comes from the C atom in the β-position with respect to the surface Zn or surface O atoms.

Within the context of the proposed mechanism, the formation of H_2O (step 6) results from the reaction of OH groups (resulting from C–O cleavage in CH_3CH_2OH) with H atoms (resulting from O–H cleavage in CH_3CH_2OH and β-hydride elimination in CH_3CH_2O– and CH_3CH_2– groups). If this were the only source of H_2O formation, then the yield of H_2O would be equal that of CH_2=CH_2. Similarly, the yield of H_2 from recombination of H atoms would be equal to the yield of CH_3CH=O. While the excess yield of H_2O (D_2O) for decomposition of CH_3CH_2OH (CD_3CD_2OD) is not statistically significant, the yields of H_2 (D_2) are clearly lower than expected. In the case of H_2O yield, the possible excess might be attributable to H_2O adsorption from the background of the UHV chamber. However, this has been ruled out by direct measurements of the H_2O adsorption from the chamber background onto the clean ZnO($1\bar{1}00$) surface; H_2O adsorption on the experimental timescale is undetectable (Figure S5 in the Supplemental Information). These observations suggest that adsorbed H atoms can reduce the surface and extract lattice O atoms to yield H_2O. This step is consistent with formation of surface OH species from adsorbed H that has been observed through vibrational spectroscopies and linked to H_2O formation from ZnO [19–21].

In addition to the product distribution and yield, the temperatures at which various reaction steps occur and at which products are observed desorbing from the surface provides some insight into the mechanism of ethanol decomposition on ZnO($1\bar{1}00$). Table 2 shows the peak locations for the acetaldehyde and ethylene species desorption during TPRS of CF_3CH_2OH, CH_3CH_2OH, and CD_3CD_2OD on ZnO($1\bar{1}00$). TPR spectra for CH_3CH=O and CD_3CD=O were best fit by two peaks while CF_3CH=O desorption was best fit by one peak. The peaks for desorption of CH_3CH=O and CD_3CD=O are, within statistical uncertainty, located at the same temperatures. The peak for desorption of CD_2=CD_2 is at a significantly higher temperature than that for CH_2=CH_2. These results reveal a significant deuterium kinetic isotope effect in CD_2=CD_2 formation, but not in CD_3CD=O formation. The isotope effect in ethylene formation suggests that C–H(D) bond breaking on the β-C atom (β-hydride elimination) is the rate limiting step in CH_3CH_2– (CD_3CD_2–) decomposition (step 5). Such isotope effects have been observed in β-hydride elimination of alkyl groups on Cu surfaces [22, 23]. Although β-hydride elimination is the expected reaction pathway for CH_3CH=O (CD_3CD=O) formation from ethoxy groups (step 2), this does not exhibit a deuterium isotope effect in the acetaldehyde desorption temperature. This is in contrast with results revealing a deuterium kinetic isotope effect during β-hydride elimination in ethoxy groups on Cu surfaces [24].

4.2 Transition states for β-elimination on ZnO($1\bar{1}00$)

The use of substituent effects is a classical approach to probing the characteristics of transitions states for elementary reactions and has been used in studies of surface chemistry on metals, and to a lesser extent oxides [24–27]. Our comparison of the decomposition of CF_3CH_2OH and CH_3CH_2OH (or CD_3CD_2OD) on ZnO($1\bar{1}00$) reveals the same decomposition products but a significant impact of F substitution on the decomposition kinetics. The key point is that the observed F substitution effects are completely consistent with the proposed decomposition via two pathways with different reaction intermediates. Figure 8 provides a direct comparison of the product desorption kinetics for CF_2=CH_2, CH_2=CH_2 and CD_2=CD_2. This reveals the small but observable deuterium kinetic isotope effect of 15 ± 7 K reported in Table 1 and attributed to β-hydride elimination from an ethyl group adsorbed at a surface O atom (step 5). This deuterium isotope effect is less well resolved than in previous studies of alkyl group decomposition by β-hydride elimination on Cu surfaces, largely because of the broad temperature range over which the reaction occurs on ZnO($1\bar{1}00$) [22, 23]. However, the magnitude of the temperature shift is similar to that reported in prior studies on Cu single crystal surfaces.

The CF_2=CH_2 product of CF_3CH_2OH decomposition on ZnO($1\bar{1}00$) desorbs at ~40 K lower temperature than CH_2=CH_2 from CH_3CH_2OH decomposition. This indicates that the barrier to β-fluoride elimination in CF_3CH_2– groups is significantly lower than that for β-hydride elimination in CH_3CH_2– groups. This is entirely consistent with the results for the same reactions on Ag(111) [28]. The F deposited onto the ZnO($1\bar{1}00$) surface by β-fluoride

Table 2 TPRS peak temperatures for aldehyde and ethylene products of CH_3CH_2OH, CD_3CD_2OD, and CF_3CH_2OH decomposition on $ZnO(1\bar{1}00)$

Reactant	Product	Peak temperature (K)	Product	Peak temperature (K)
CH_3CH_2OH	$CH_3CH{=}O$ (low T)	436 ± 4	$CH_2{=}CH_2$	468 ± 5
	$CH_3CH{=}O$ (high T)	491 ± 7		
CD_3CD_2OD	$CD_3CD{=}O$ (low T)	435 ± 8	$CD_2{=}CD_2$	487 ± 5
	$CD_3CD{=}O$ (high T)	491 ± 3		
CF_3CH_2OH	$CF_3CH{=}O$	562 ± 4	$CF_2{=}CH_2$	428 ± 10

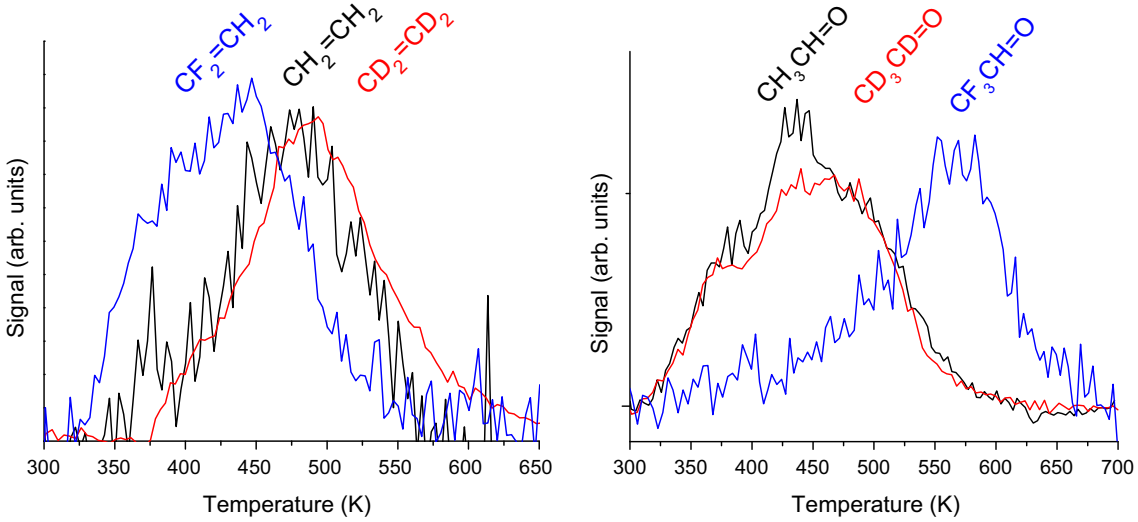

Fig. 8 TPR spectra of ethylene (*left*) and aldehyde (*right*) desorption following saturation exposures of CH_3CH_2OH, CD_3CD_2OD, and CF_3CH_2OH to the $ZnO(1\bar{1}00)$ surface. The data from $CF_2{=}CH_2$ and $CF_3CH{=}O$ is not in units of pressure and is divided by 30 for comparing peak locations. F substitution into the ethanol lowers the temperature of the ethylene formation and desorption and raises the temperature of acetaldehyde formation and desorption

elimination is detected in XPS after reaction completion (Fig. 7). Because the C–F bond is ~80–100 kJ/mole stronger than a C–H bond [29], the lower barrier to β-fluoride elimination must arise from a stronger interaction of the $ZnO(1\bar{1}00)$ surface with the product F atom than with a H atom.

Finally, Fig. 8 reveals that the temperature at which $CF_3CH{=}O$ appears during CF_3CH_2OH decomposition on $ZnO(1\bar{1}00)$ is ~100 K higher than that of $CH_3CH{=}O$ appearance during CH_3CH_2OH decomposition. This is entirely consistent with F substitution effects observed for decomposition of ethoxy groups by β-hydride elimination on Cu single crystal surfaces [24, 30–33]. In those studies and as modeled by DFT calculations, this increase in the barrier to β-hydride elimination is associated with a transition state in which the C atom adjacent to the CF_3– substituent group is cationic with respect to its initial state in the ethoxy group, $R{-}C{-}H \rightarrow \left[R{-}C^{\delta+}\cdots H^{\delta-}\right]^{\ddagger}$. Substitution of $R{=}CF_3$ for CH_3 results in inductive destabilization of the cationic transition state as a result of the strong polarity of the $F^{\delta-} - C^{\delta+}$ bonds adjacent to the β-hydride elimination reaction center. Similar F substituent effects have been observed for CF_3CH_2OH decomposition on vanadia surfaces [27]. The net observations of F substituent effects on the decomposition of ethanol to both ethylene and to acetaldehyde are consistent with a mechanism in which there are two distinct intermediates; an ethyl group that leads to the formation of ethylene and an ethoxy group that leads to the formation of acetaldehyde, both by β-hydride elimination.

5 Conclusions

The decomposition of CH_3CH_2OH, CD_3CD_2OD, and CF_3CH_2OH was studied on a $ZnO(1\bar{1}00)$ single crystal using TPRS and XPS analysis. All three adsorbates display both reversible desorption and decomposition to yield acetaldehyde, ethylene, water and hydrogen. Quantitative analysis of the desorbing species was used to determine the product ratios of CH_3CH_2OH and CD_3CD_2OD decomposition. The products yields, the deuterium isotope effects and the F substituent effects on the reaction kinetics demonstrate that the decomposition reaction mechanism is one in which there are two competing pathways. Ethanol

deprotonation (O–H scission) to yield ethoxy results in the formation of acetaldehyde. Ethanol dehydroxylation (C–OH scission) to yield ethyl groups results in the formation of ethylene. By analogy with suggestions based on STM imaging of CH_3OH adsorption on ZnO($1\bar{1}00$), we suggest that the ethoxy groups are formed on surface lattice Zn sites while the ethyl groups are formed on surface lattice O sites.

Acknowledgments We acknowledge support from the National Research Foundation of Korea under Grant Number KSF GRNP 220-2011-1-C00033.

References

1. Behrens M, Studt F, Kasatkin I, Kuhl S, Havecker M, Abild-Pedersen F, Zander S, Girgsdies F, Kurr P, Kniep BL, Tovar M, Fischer RW, Norskov JK, Schlogl R (2012) The active site of methanol synthesis over Cu/ZnO/Al_2O_3 industrial catalysts. Science 336(6083):893–897
2. Cui Y, Wei QQ, Park HK, Lieber CM (2001) Nanowire nanosensors for highly sensitive and selective detection of biological and chemical species. Science 293(5533):1289–1292
3. Cui Y, Zhong ZH, Wang DL, Wang WU, Lieber CM (2003) High performance silicon nanowire field effect transistors. Nano Lett 3(2):149–152
4. Banerjee D, Jo SH, Ren ZF (2004) Enhanced field emission of ZnO nanowires. Adv Mater 16(22):2028
5. Law M, Greene LE, Johnson JC, Saykally R, Yang PD (2005) Nanowire dye-sensitized solar cells. Nat Mater 4(6):455–459
6. Mokwa W, Kohl D, Heiland G (1982) Decomposition of ethanol and acetaldehyde on clean ZnO prism and oxygen faces. Surf Sci 117(1–3):659–667
7. Cheng WH, Akhter S, Kung HH (1983) Structure sensitivity in methanol decomposition on ZnO single crystal surfaces. J Catal 82(2):341–350
8. Akhter S, Cheng WH, Lui K, Kung HH (1984) Decomposition of methanol, formaldehyde, and formic-acid on nonpolar (1,0,-1,0), stepped (5,0,-5,1), and (0001) surfaces of ZnO by temperature-programmed decomposition. J Catal 85(2):437–456
9. Zwicker G, Jacobil K, Cunningham J (1984) Temperature programmed desorption of polar adsorbates from (1010), (0001) and (0001) ZnO surfaces. Int J Mass Spectrom Ion Process 60(1):213–223
10. Mokwa W, Kohl D, Heiland G (1983) Decomposition of ethanol on Cu-Zno and Pd-Zno. Fresenius Zeitschrift Fur Analytische Chemie 314(3):315–318
11. Kwak G, Yong KJ (2008) Adsorption and reaction of ethanol on ZnO nanowires. J Phys Chem C 112(8):3036–3041
12. Martono E, Hyman MP, Vohs JM (2011) Reaction pathways for ethanol on model Co/ZnO(0001) catalysts. Phys Chem Chem Phys 13(20):9880–9886
13. Shao X, Fukui K, Kondoh H, Shionoya M, Iwasawa Y (2009) Stm study of surface species formed by methanol adsorption on stoichiometric and reduced ZnO(1,0,-1,0) surfaces. J Phys Chem C 113(32):14356–14362
14. Dulub O, Boatner LA, Diebold U (2002) Stm study of the geometric and electronic structure of ZnO(0001)-Zn, (0,0,0,-1)-O, (1,0,-1,0), and (1,1,-2,0) surfaces. Surf Sci 519(3):201–217
15. C. D. Wagner, A. V. N., A. Kraut-Vass, J. W. Allison, C. J. Powell, J. R. Rumble NIST XPS Database. http://srdata.nist.gov/xps/
16. Taemm K, Mayeux C, Sikk L, Gal J-F, Burk P (2013) Theoretical modeling of sensitivity factors of Bayard-Alpert ionization gauges. Int J Mass Spectrom 341:52–58
17. Tawarah KM, Hansen RS (1984) Kinetics and mechanism of methanol decomposition over Zinc-Oxide. J Catal 87(2):305–318
18. Vest MA, Lui KC, Kung HH (1989) Catalytic decomposition of methanol on ZnO single crystal surfaces at low and near atmospheric pressures. J Catal 120(1):231–255
19. Shi GA, Stavola M, Pearton SJ, Thieme M, Lavrov EV, Weber J (2005) Hydrogen local modes and shallow donors in ZnO. Phys Rev B 72(19):195211
20. Yin XL, Birkner A, Hanel K, Lober T, Kohler U, Woll C (2006) Adsorption of atomic hydrogen on ZnO(1010): stm study. Phys Chem Chem Phys 8(13):1477–1481
21. Wong KW, Field MR, Ou JZ, Latham K, Spencer MJ, Yarovsky I, Kalantar-zadeh K (2012) Interaction of hydrogen with ZnO nanopowders—evidence of hydroxyl group formation. Nanotechnology 23(1):015705
22. Jenks CJ, Bent BE, Bernstein N, Zaera F (1993) Chemistry of 1-Iodopropane on Cu(110)—formation, bonding, and reaction of adsorbed Propyl groups. J Am Chem Soc 115(1):308–314
23. Teplyakov AV, Bent BE (1995) Distinguishing direct and quasi-direct mechanisms for an Eley-Rideal gas/surface reaction. Stereochemistry of H addition to cyclohexene on Cu (100). J Chem Soc Faraday Trans 91(20):3645–3654
24. Gellman AJ, Buelow MT, Street SC, Morton TH (2000) Transition state for B-elimination of hydrogen from alkoxy groups on metal surfaces. J Phys Chem A 104(11):2476–2485
25. Gellman AJ (2002) The influence of catalytic surfaces on the barriers to elementary surface reaction steps. J Phys Chem B 106(41):10509–10517
26. Gellman AJ (2000) Transition states for surface-catalyzed chemistry. Acc Chem Res 33(1):19–26
27. Feng T, Vohs JM (2004) Mechanism of β-hydrogen abstraction from adsorbed alkoxides on supported metal oxide catalysts. J Phys Chem B 108(18):5647–5652
28. Paul A, Gellman AJ (1995) β-Fluoride Elimination Reactions of Fluorinated Alkyl Group on the Ag(111) Surface. Langmuir 11(11):4433–4439
29. deB Darwent B (1970) Bond Dissocaition Energies in Simple Molecules. National Standard Reference Data System, vol 31. US National Bureau of Standards, Washington, DC
30. Li X, Gellman AJ, Sholl DS (2006) Using β-hydride elimination to test propositions for characterizing surface catalyzed reactions. Surf Sci 600(3):L25–L28
31. Gellman AJ, Dai Q (1993) Mechanism of β-hydride elimination in adsorbed alkoxides. J Am Chem Soc 115(2):714–722
32. Forbes JG, Gellman AJ (1993) The β-hydride elimination mechanism in adsorbed alkyl groups. J Am Chem Soc 115(14):6277–6283
33. Dai Q, Gellman AJ (1993) Fluorine substituent effects on alkoxide chemistry and orientation on the Cu(100) surface. J Phys Chem 97(41):10783–10789